Supplementary Information

Surface engineering of stainless-steel mesh with superwettability toward efficient water treatment through electroflotation

Junkai Ma,†[abc] Liwei Fu,†[bcd] Yanan Chen,[bc] Shaoqing Zhu,[e] Yaofang Fan*[a], Wenshuo Wang*[bc]

a. College of Biological Engineering, Qingdao University of Science and Technology, Qingdao 266042, China. E-mail: fanyfz6@163.com

b. Qingdao Institute of Bioenergy and Bioprocess Technology, Chinese Academy of Sciences, Qingdao 266101, China. E-mail: wangws@qibebt.ac.cn

c. Shandong Energy Institute, Qingdao 266101, China.

d. College of Chemistry and Chemical Engineering, Qingdao University, Qingdao 266071, China.

e. Weichai Power Co., Ltd.

† Junkai Ma and Liwei Fu contributed equally to this work.

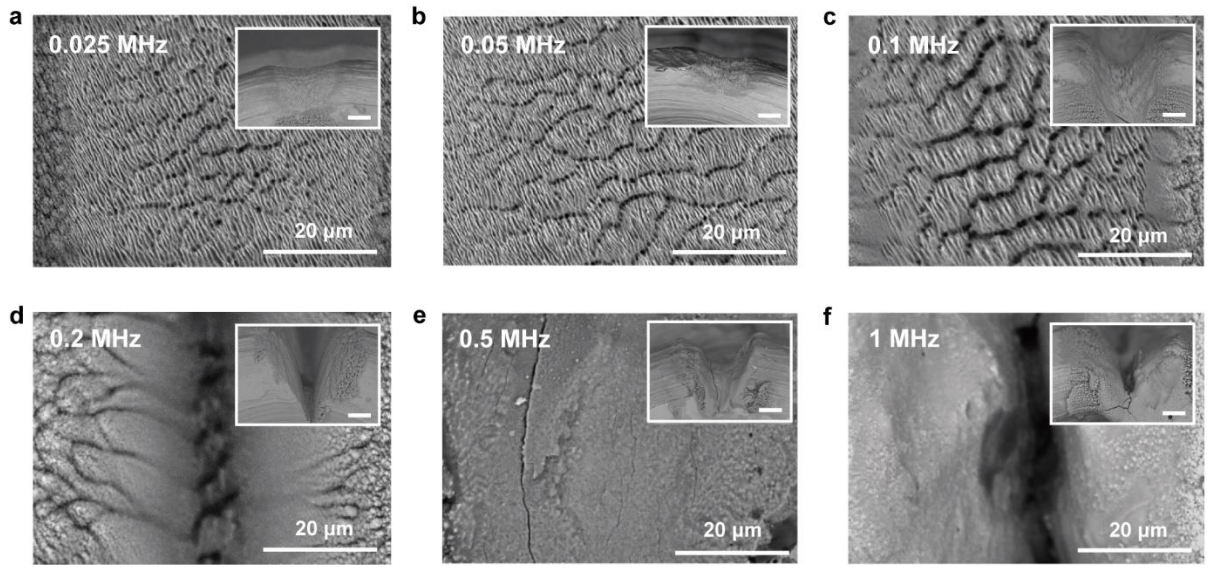

Fig. S1. Morphological characterization of LSS under laser-ablated with different repetition frequency ranging from 0.025 MHz to 1 MHz. The results indicate that as the repetition frequency increases, the laser-induced grooves become deeper, whereas the nanoscale ripples gradually diminish and eventually disappear. To simultaneously achieve sufficient groove depth and well-defined nanoscale ripples, a repetition frequency of 0.1 MHz was selected as the optimal parameter.

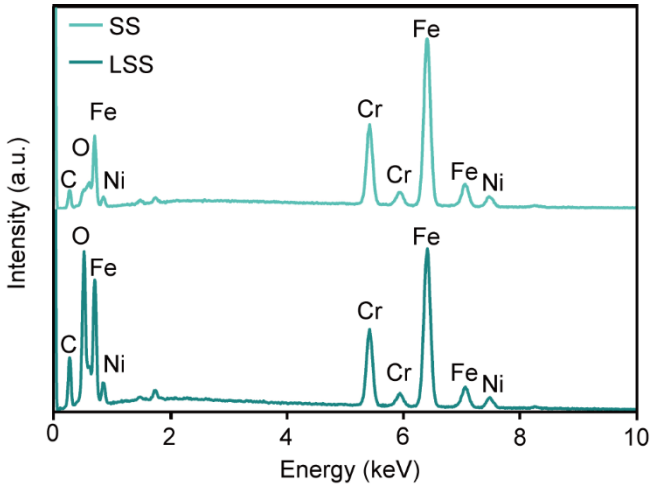

Fig. S2. Elemental compositions of stainless steel meshes before and after laser ablation.

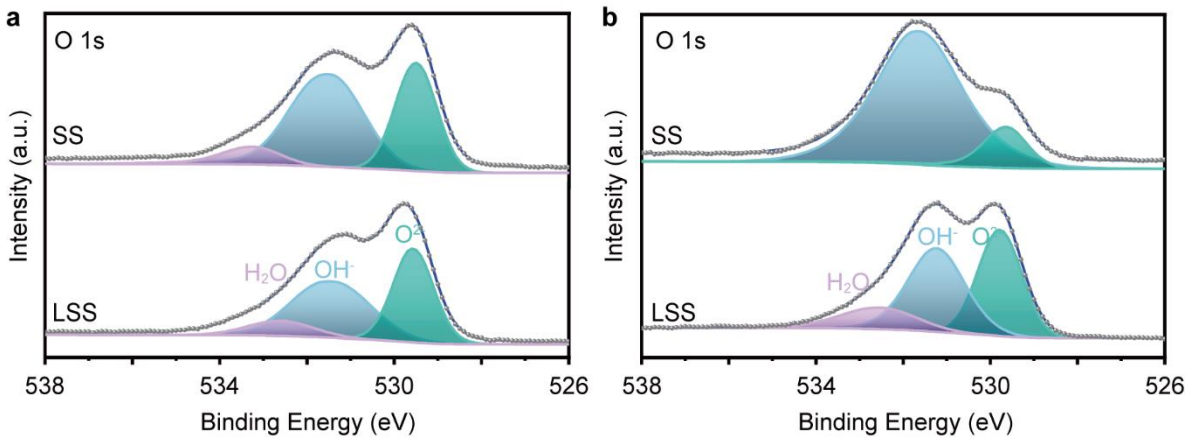

Fig. S3. XPS spectra of O 1s of the SS and the LSS before (a) and after (b) electrochemical test for HER at voltage of -0.59 V vs. RHE.

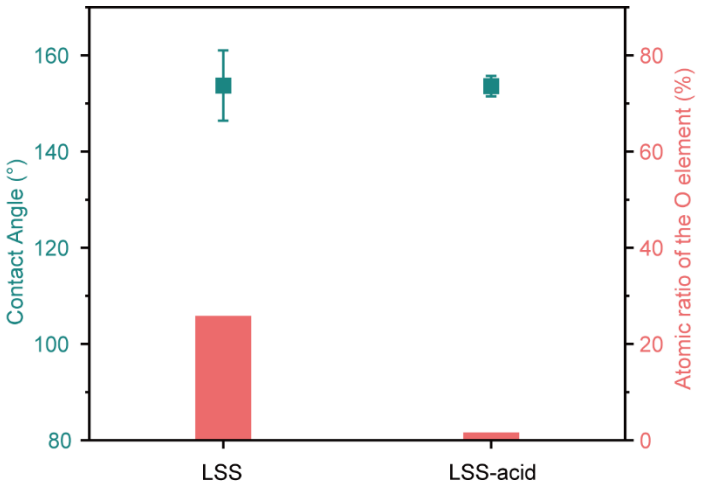

Fig. S4. Underwater bubble contact angle of the LSS electrode before and after treatment with 0.5 M hydrochloric acid to remove surface oxides.

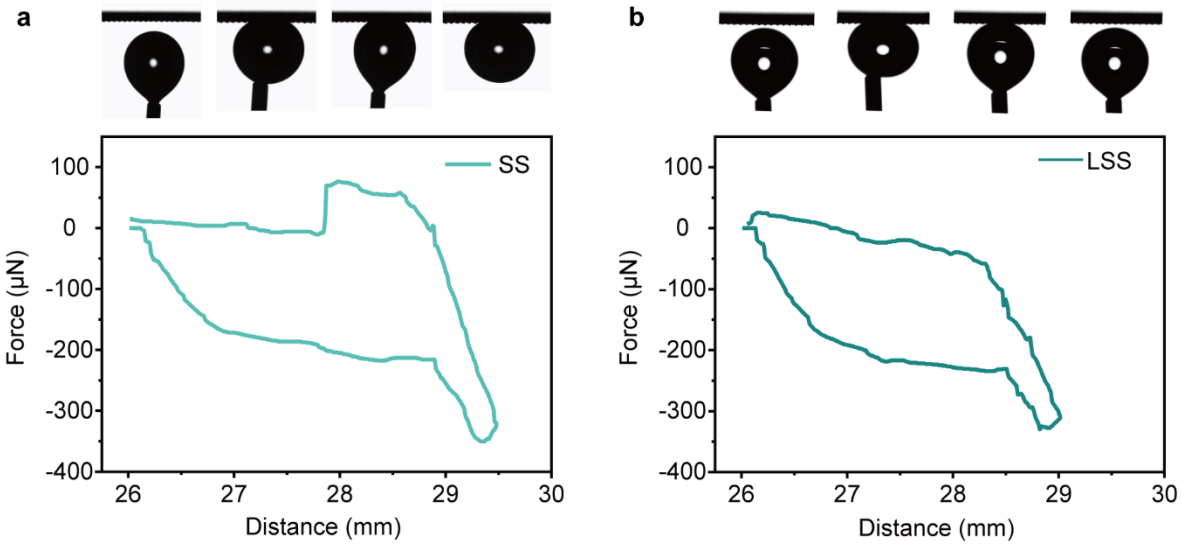

Fig. S5. Bubble adhesion measurements on the original SS (a) and on the laser-ablated SS (b).

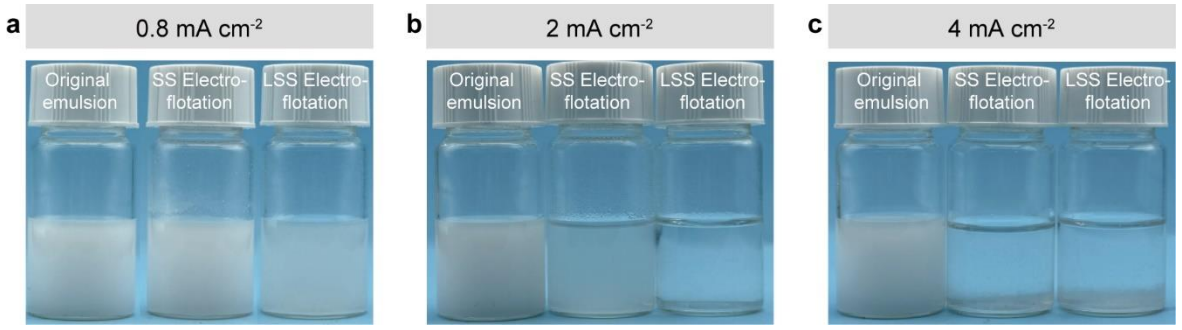

Fig. S6. Photographs of the oily water before (left) and after electroflotation by the SS electrode (middle) and by the LSS electrode (right) for 50 min at current density of 0.8 mA cm^{-2} (a), 2 mA cm^{-2} (b), and 4 mA cm^{-2} (c).

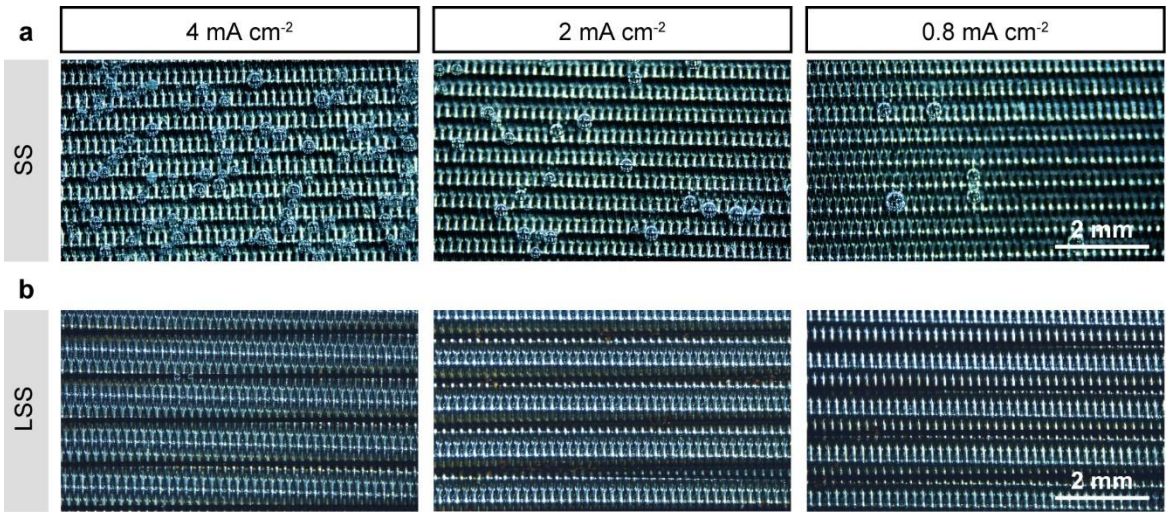

Fig. S7. Photographs of adhered bubbles on the SS electrode and on the LSS electrode under different current densities.

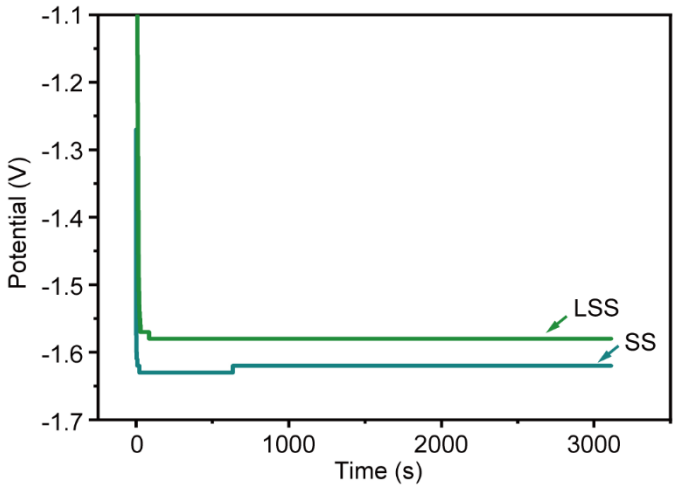

Fig. S8. The voltage curves during electroflotation for the SS electrode and the LSS electrode at 2 mA cm^{-2}.

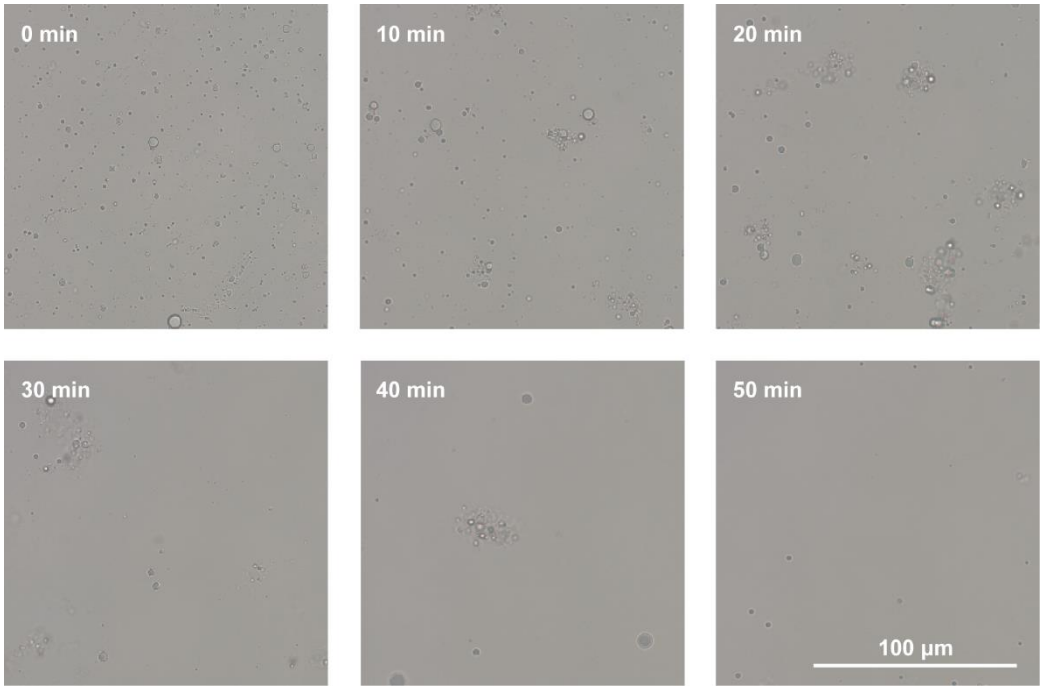

Fig. S9. Optical images of oil droplets in oily water during electroflotation by the SS electrode at 2 mA cm^{-2}.

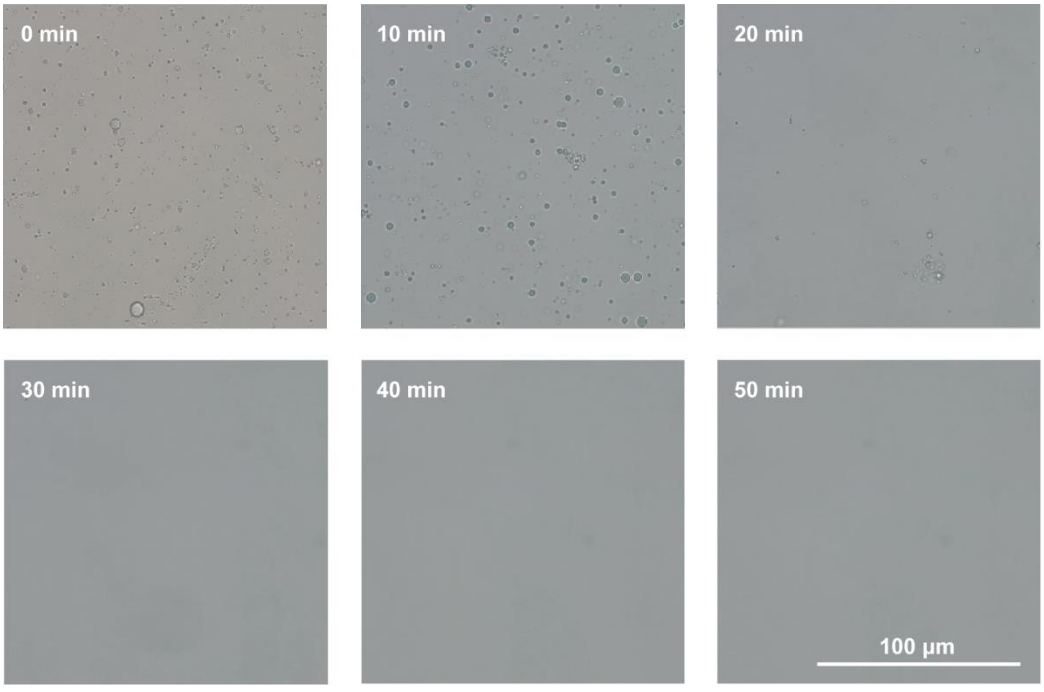

Fig. S10. Optical images of oil droplets in oily water during electroflotation by the LSS electrode at 2 mA cm^{-2}.

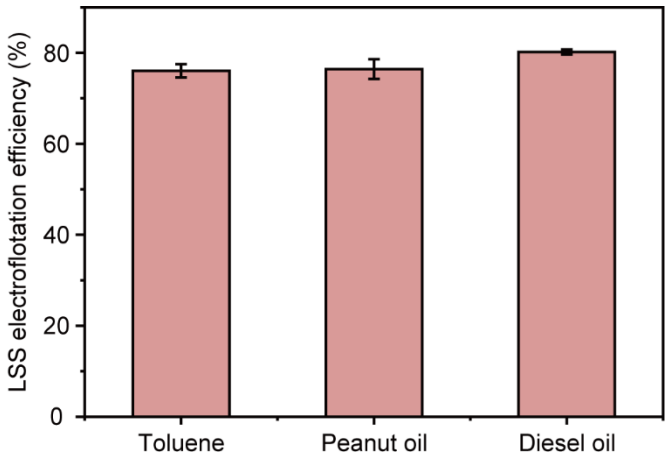

Fig. S11. Electroflotation of toluene, peanut oil, and diesel emulsions by the LSS electrode at 2 mA cm^{-2} for 50 min.

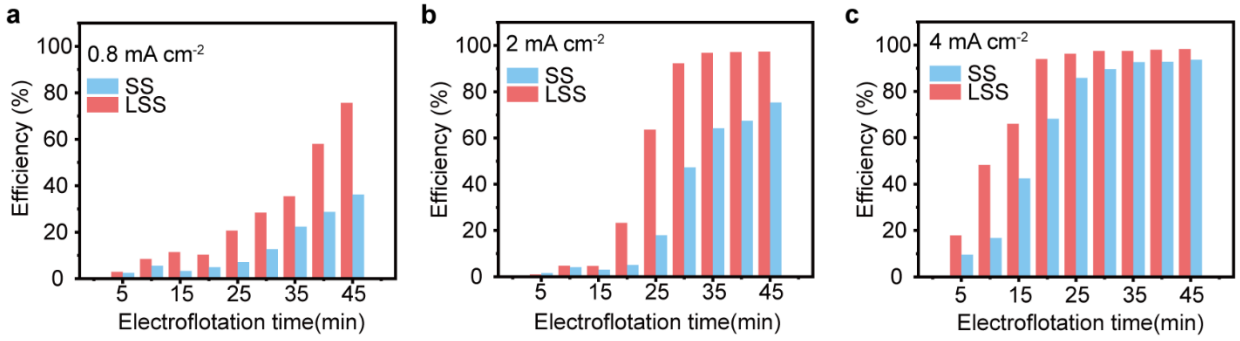

Fig. S12. Electroflotation to remove bacteria *S. aureus* by the SS electrode and the LSS electrode at 0.8 mA cm^{-2} (a), 2 mA cm^{-2} (b), 4 mA cm^{-2} (c).

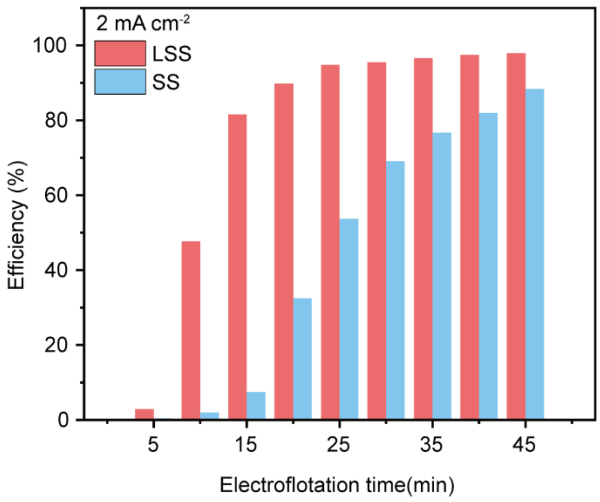

Fig. S13. Electroflotation to remove bacteria E. coli by the SS electrode and the LSS electrode at 2 mA cm^{-2}.

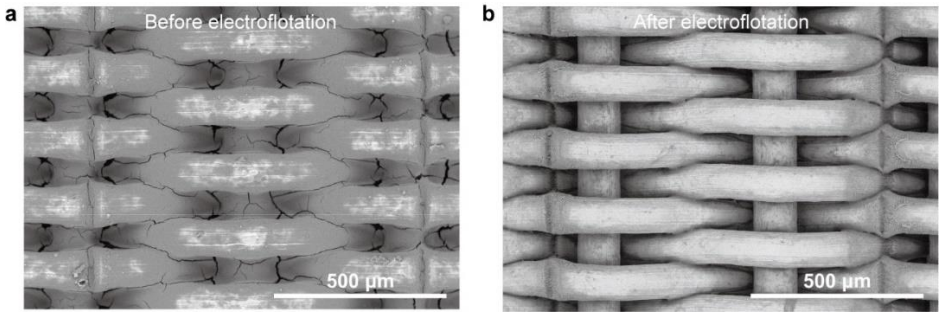

Fig. S14. Antifouling test. The efficient removal of adhered bacteria E. coli by electroflotation at 2 mA cm^{-2} for 5 min indicates the robust antifouling performance of the LSS electrode.